AUG 15 1997

ORNL
Master Copy

NUREG/CR-6454
ORNL/TM-13205

Pool Critical Assembly Pressure Vessel Facility Benchmark

Prepared by
I. Remec, F. B. K. Kam

Oak Ridge National Laboratory

Prepared for
U.S. Nuclear Regulatory Commission

AVAILABILITY NOTICE

Availability of Reference Materials Cited in NRC Publications

Most documents cited in NRC publications will be available from one of the following sources:

1. The NRC Public Document Room, 2120 L Street, NW., Lower Level, Washington, DC 20555-0001

2. The Superintendent of Documents, U.S. Government Printing Office, P. O. Box 37082, Washington, DC 20402-9328

3. The National Technical Information Service, Springfield, VA 22161-0002

Although the listing that follows represents the majority of documents cited in NRC publications, it is not intended to be exhaustive.

Referenced documents available for inspection and copying for a fee from the NRC Public Document Room include NRC correspondence and internal NRC memoranda; NRC bulletins, circulars, information notices, inspection and investigation notices; licensee event reports; vendor reports and correspondence; Commission papers; and applicant and licensee documents and correspondence.

The following documents in the NUREG series are available for purchase from the Government Printing Office: formal NRC staff and contractor reports, NRC-sponsored conference proceedings, international agreement reports, grantee reports, and NRC booklets and brochures. Also available are regulatory guides, NRC regulations in the *Code of Federal Regulations*, and *Nuclear Regulatory Commission Issuances*.

Documents available from the National Technical Information Service include NUREG-series reports and technical reports prepared by other Federal agencies and reports prepared by the Atomic Energy Commission, forerunner agency to the Nuclear Regulatory Commission.

Documents available from public and special technical libraries include all open literature items, such as books, journal articles, and transactions. *Federal Register* notices, Federal and State legislation, and congressional reports can usually be obtained from these libraries.

Documents such as theses, dissertations, foreign reports and translations, and non-NRC conference proceedings are available for purchase from the organization sponsoring the publication cited.

Single copies of NRC draft reports are available free, to the extent of supply, upon written request to the Office of Administration, Distribution and Mail Services Section, U.S. Nuclear Regulatory Commission, Washington, DC 20555-0001.

Copies of industry codes and standards used in a substantive manner in the NRC regulatory process are maintained at the NRC Library, Two White Flint North, 11545 Rockville Pike, Rockville, MD 20852-2738, for use by the public. Codes and standards are usually copyrighted and may be purchased from the originating organization or, if they are American National Standards, from the American National Standards Institute, 1430 Broadway, New York, NY 10018-3308.

DISCLAIMER NOTICE

This report was prepared as an account of work sponsored by an agency of the United States Government. Neither the United States Government nor any agency thereof, nor any of their employees, makes any warranty, expressed or implied, or assumes any legal liability or responsibility for any third party's use, or the results of such use, of any information, apparatus, product, or process disclosed in this report, or represents that its use by such third party would not infringe privately owned rights.

NUREG/CR-6454
ORNL/TM-13205

Pool Critical Assembly Pressure Vessel Facility Benchmark

Manuscript Completed: July 1996
Date Published: July 1997

Prepared by
I. Remec, F. B. K. Kam

Oak Ridge National Laboratory
Managed by Lockheed Martin Energy Research Corp.

Oak Ridge National Laboratory
Oak Ridge, TN 37831-6370

C. J. Fairbanks, NRC Project Manager

Prepared for
Division of Engineering Technology
Office of Nuclear Regulatory Research
U.S. Nuclear Regulatory Commission
Washington, DC 20555-0001
NRC Job Code W6164

NUREG/CR-6454 has been reproduced
from the best available copy.

ABSTRACT

The pool critical assembly (PCA) pressure vessel wall facility benchmark (PCA benchmark) is described and analyzed in this report. Analysis of the PCA benchmark can be used for partial fulfillment of the requirements for the qualification of the methodology for pressure vessel neutron fluence calculations, as required by the U.S. Nuclear Regulatory Commission regulatory guide DG-1053 "Calculational and Dosimetry Methods for Determining Pressure Vessel Neutron Fluence."

Section 1 of this report describes the PCA benchmark and provides all the dimensions, material compositions and neutron source data necessary for the benchmark analysis. The measured quantities, to be compared with the calculated values, are the equivalent fission fluxes. The characteristic feature of the PCA benchmark is that it provides measurements inside the simulated pressure vessel, therefore allowing an assessment of the accuracy of the calculations within the pressure vessel.

In Section 2 the analysis of the PCA benchmark is described. Calculations with the computer code DORT, based on the discrete-ordinates method, were performed for three ENDF/B-VI- based multigroup libraries: BUGLE-93, SAILOR-95, and BUGLE-96. An excellent agreement of the calculated (C) and measured (M) equivalent fission fluxes was obtained. The average C/M for all the dosimeters (total of 31) was 0.93 ± 0.03 and 0.92 ± 0.03 for the SAILOR-95 and BUGLE-96 libraries, respectively. The BUGLE-93 library significantly overpredicted the thermal neutron fluxes and consequently the neptunium fission rates in water and air regions. The average C/M ratio, obtained with the BUGLE-93 library, for all the measurements except the neptunium measurements in the water and air regions (a total of 28 measurements) was 0.93 ± 0.03. No systematic decrease in the C/M ratios with increasing distance from the core was observed for any of the libraries used. It is expected that the agreements of the calculations with the measurements, similar to those obtained in this report, should typically be observed when the discrete-ordinates method and ENDF/B-VI libraries are used for the PCA benchmark analysis.

CONTENTS

ABSTRACT iii
LIST OF FIGURES vii
LIST OF TABLES ix
ACKNOWLEDGEMENTS xi

1 BENCHMARK DEFINITION 1
1.1 INTRODUCTION 1
1.2 DESCRIPTION 1
1.3 MEASUREMENT RESULTS 4
1.4 REFERENCE 5

2 BENCHMARK ANALYSIS 22
2.1 METHODOLOGY 22
2.2 RESULTS AND DISCUSSION 24
2.3 REFERENCES 30

3 CONCLUSION 31

APPENDIX A 33
REFERENCE 35

LIST OF FIGURES

Fig. 1.1 PCA pressure vessel wall benchmark facility 11
Fig. 1.2 Horizontal cross section of the PCA pressure vessel benchmark facility 12/13 configuration 12
Fig. 1.3 Vertical cross section of the PCA pressure vessel benchmark facility 13
Fig. 1.4 Detail of the interface of the PCA fuel cell boundary and the core aluminum window 14
Fig. 1.5 Fuel loading pattern for the PCA-pressure vessel experiment 15
Fig. 1.6 Cross section of the standard PCA fuel element with 18 fuel plates 16
Fig. 1.7 Depiction of the aluminum side plates, taken from drawing D-7207 ("Fuel & Side Plates"), for the standard fuel element (*top*) and control-rod fuel element (*bottom*) 17
Fig. 1.8 Details of the standard fuel plate, taken from drawing D-7207 ("Fuel & Side Plates") 18
Fig. 1.9 Horizontal cross section (through the fueled region) of the control-rod fuel element taken from drawing D-7206 ("Special Fuel Element for Control Rod") 19
Fig. 1.10 Coordinate system used for description of PCA core power distribution 20
Fig. 1.11 Relative fuel element powers 21

LIST OF TABLES

Table 1.1 Dimensions of PCA components outside the core 5
Table 1.2 Material specifications for PCA components outside the core 5
Table 1.3 PCA fuel elements 6
Table 1.4 Selected data on PCA core and fuel elements 7
Table 1.5 Horizontal relative power density distribution 9
Table 1.6 Experimental results for fission chamber and radiometric measurements of equivalent fission fluxes 10
Table 2.1 Comparison of the reaction rates obtained from the calculations with BUGLE-93, SAILOR-95, and BUGLE-96 cross sections for transport calculations 25
Table 2.2 Ratios of calculated-to-measured (C/M) equivalent fission fluxes obtained by the BUGLE-93 library 27
Table 2.3 Ratios of calculated-to-measured (C/M) equivalent fission fluxes obtained by the SAILOR-95 library 28
Table 2.4 Ratios of calculated-to-measured (C/M) equivalent fission fluxes obtained by the BUGLE-96 library 28
Table A.1 Comparison of the reaction rates calculated with different sets of dosimetry cross-sections 35
Table A.2 Comparison of the reaction rates calculated using different modeling approximations 37

ACKNOWLEDGEMENTS

The authors wish to express their appreciation to the reviewers, Joe V. Pace III from the Oak Ridge National Laboratory and Mark L. Williams from the Louisiana State University Nuclear Science Center, for their comments and suggestions. Special thanks goes to Carolyn Moser for providing the editorial review and Tamara Henson for the preparation of this reports. Finally, the authors gratefully acknowledge the programmatic support and encouragement from Al Taboada, Carolyn Fairbanks, and Mike Mayfield of the Nuclear Regulatory Commission. This support was essential for accomplishing our objectives.

1 BENCHMARK DEFINITION

1.1 INTRODUCTION

This section defines the pool critical assembly (PCA) pressure vessel wall facility benchmark. Analysis of the PCA benchmark can be used for partial fulfillment of the requirements for the qualification of the methodology for pressure vessel neutron fluence calculations, as required by the U.S. Nuclear Regulatory Commission Regulatory Guide DG-1053[1].

The scope of the PCA benchmark is to validate the capabilities of the calculational methodology to predict the reaction rates in the region outside the core when the neutron source, material compositions, and relatively simple geometry configuration are well defined and given. The characteristic feature of the PCA benchmark is that it provides measured reaction rates inside the simulated pressure vessel, as well as in the water gap in front of the pressure vessel. This allows an assessment of the accuracy with which the calculations predict the neutron flux attenuation inside the pressure vessel.

Measured quantities, used in the PCA benchmark, are given in terms of the equivalent ^{235}U fission fluxes. To complete the PCA benchmark analysis the analyst must determine the calculated-to-measured (C/M) ratios of the equivalent ^{235}U fission fluxes for all the locations and all the dosimeters for which the measured values are provided.

Section 1 of this document provides all data, geometry layout, material composition, and neutron source, that are required to perform the PCA benchmark analysis. Reference to the document with more detailed information is provided, but this document is not necessary for the benchmark calculation.

It is estimated that an experienced analyst using established calculational methodology (including computer codes, neutron transport, and dosimetry cross sections) can complete the PCA benchmark analysis in approximately 40 man-hours or less.

1.2 DESCRIPTION

An overall view of the PCA pressure vessel wall benchmark facility is shown in Fig. 1.1. The facility consists of the PCA reactor core and the components that mock up the core-to-cavity region in light water reactors (LWRs). These components are the thermal shield (TS), the pressure vessel simulator (PVS) and the void box (VB), which simulates the reactor cavity. An aluminum plate, referred to in Fig. 1.1 as the reactor window simulator, was added to the facility for operational reasons (Ref. 1). The thicknesses of the water gaps between the aluminum window and thermal shield, and between

---

[1]U.S. Nuclear Regulatory Commission, "Calculational and Dosimetry Methods for Determining Pressure Vessel Neutron Fluence, "Draft Regulatory Guide DG-1053, to be published.

the thermal shield and pressure vessel, are approximately 12 cm and 13 cm, respectively. For this reason this configuration was labeled a 12/13 configuration.[2] The as-built dimensions are given in Fig. 1.2, which shows the horizontal cross section, and Fig. 1.3, which shows the vertical cross section. A detail of the interface of the PCA fuel cell boundary and the aluminum window is shown in Fig. 1.4. The dimensions of the components outside the core are listed in Table 1.1. The materials used for the components outside the core were aluminum for the reactor window simulator, stainless steel for the thermal shield, and carbon steel for the pressure vessel. The densities and chemical compositions for these materials are given in Table 1.2. The facility is located in a large pool of water, which serves as reactor core coolant and moderator and provides shielding. The water temperature is approximately 37.7°C; however, there is a 5°C fluctuation of water temperature from summer to winter.

The PCA core is a light-water-moderated, enriched-uranium-fueled critical assembly. It consists of 25 material test reactor (MTR) plate-type elements. The fuel loading pattern used for the PCA pressure vessel wall benchmark facility experiments was carefully chosen to satisfy the following requirements:

1. The fuel elements must contain essentially no fission products
2. The fuel elements on the first row facing the experiment must be of the same type and must contain equal masses of ^{235}U
3. Quarter-core symmetry must be maintained
4. The core must be critical with the control rods withdrawn more than 45.72 cm (18 in.)[3]
5. A fuel element must be inserted at core center with a missing fuel plate to permit run-to-run power normalization.[4]

The fuel loading pattern shown in Fig. 1.5 was assumed to satisfy all the requirements (including requirement 4), since the regulating rod is worth a small fraction of the three safety rods. Tables 1.3 and 1.4 provide essential data on the PCA core and fuel elements. Views of the fuel element, side plates, fuel plate, and special fuel element for control rod are shown in Figs. 1.6-1.9.

---

[2]Experiments were performed in four different PCA PV configurations: 8/7, 12/13, 4/12, and 4/12 with simulated surveillance capsule. For the benchmark described in this report, the 12/13 configuration was selected.

[3]The fully inserted control rod reaches to the bottom of the fuel. The withdrawn length is measured from the bottom of the fuel. The fully withdrawn position of the safety rods is 61 cm (24 in.)—that is, 0.95 cm above the top of the fueled region of the fuel element. The fully withdrawn position of the regulating rod is 56.4 cm (22.2 in.)—that is, 3.62 cm below the top of the fueled region. This information is not necessary for the benchmark calculation and is included for the sake of completeness only.

[4]This information is not necessary for the benchmark calculation and is included for the sake of completeness only.

Fig. 1.10 shows the coordinate system that is used in the description of the PCA core power distribution. The origin of the coordinate system is placed at the intersection of the aluminum window surface facing the core and the extension of the core centerline.

The PCA power distribution was carefully characterized using a combination of fission chamber measurements and core calculations (Ref. 1). The core relative power density distribution, $p(x,y,z)$, is described as a product of cosine-shaped distribution in the vertical (Z-axis) direction and a two-dimensional distribution, $p(x,y)$, which describes variations in the horizontal plane:

$$p(x,y,z) = (1/C)\ p(x,y)\ \cos[B_z(z - z_0)]\ , \tag{1.1}$$

where

$B_z =$ core average buckling,
$z_0 =$ displacement of maximum of the vertical (Z-axis) distribution from core midplane,
$C =$ normalization constant,

and

$B_z =$ $4.42\ 10^{-2}\ \mathrm{cm}^{-1}$,
$z_0 =$ -4.20 cm.

The maximum of the axial distribution lies slightly below the core horizontal midplane because the control rods are partly inserted from the top of the core.

The core horizontal power distribution $p(x,y)$ is symmetric across the X-axis; therefore, only values for one-half of the core need to be specified. Fig. 1.11 gives relative fuel element powers,[5] with values normalized to the core-average fuel element power of 1.00. For the quarter of the core closer to the aluminum window, Table 1.5 supplies the relative power densities $p(x_i,y_i)$ at selected locations (x_i,y_i).[6] Nine values per fuel element are provided. (The element at B6 contains the control rod; therefore, some power densities in it are zero).

---

[5]The relative fuel element powers were obtained from calculations (Ref. 1).

[6]Values are based on fission-chamber measurements and calculations. At locations where measurements were not available, the calculated values are given.

If the power densities given in Table 1.5 are numerically integrated over the fuel elements using appropriate weights,[7] the resulting element powers do not exactly match the powers given in Fig. 1.11. Differences vary from element to element and range from approximately 0.5% to 5%, except for the element containing the control rod, where differences of approximately 12% are found for the portion farther from the aluminum window. The total power of the nine fuel elements obtained by the integration of values in Table 1.5 is about 1.3% lower than the sum of the powers of the corresponding elements from Fig. 1.11. These differences arise from two sources: (1) the values in Fig. 1.11 are based on calculations only, whereas most of the values in Table 1.5 were obtained from the measurements; (2) the $p(x_i,y_i)$ are relative power densities at specified locations (x_i,y_i) and are not averaged over parts of the fuel element cross section, as is assumed in numerical integration. The procedure to be used to prepare the core source distribution from the data given is to be selected by the analyst.[8]

All measured quantities provided for comparison with calculated values are given per unit PCA core neutron source. Therefore, the calculated responses need to be normalized to the source strength of one fission neutron per second being born in the whole PCA core. For this reason the normalization constant C in Eq. (1.1) is not specified. The analyst needs to ensure proper source normalization.

1.3 MEASUREMENT RESULTS

Measurements were performed at core midplane (that is at $z = 0$ and $y = 0$) at several locations, labeled in Fig. 1.2 as A1 to A7. The experimental access tubes in which the measurements were done were filled with appropriate material (steel in the pressure vessel locations and Plexiglas in the in-water locations) in order to minimize the perturbations of the neutron field. For the purpose of the benchmark analysis, measurements can therefore be considered as having been done in the unperturbed medium.

---

[7]The fuel element has a horizontal cross section, S, of 7.71 × 8.10 cm, and the fuel is contained in an area, S_f, of approximately 6.27 × 7.95 cm. A weight of S_f/ 9 can be used for numerical integration of the power densities in Table 1.5. Different weights need to be used for the fuel element with control rod, where the fueled region closer to the aluminum window occupies approximately 23% of the fuel-element cross section; the control rod, 43%, and the second fueled region, 34% (see Fig. 1.9).

[8]Several approaches were investigated (see Appendix A of this report), and it was found that the variations in the reaction rates do not exceed approximately 2%.

1.4 REFERENCE

1. W. N. McElroy, ed., *LWR Pressure Vessel Surveillance Dosimetry Improvement Program: PCA Experiments and Blind Test*, NUREG/CR-1861 (HEDL-TME 80-87, R5), July 1981.

Table 1.1 Dimensions of PCA components outside the core

Component	Thickness (cm)	Width (cm)	Height (cm)
Aluminum window	2.5	91.44	89.535
Thermal shield (TS)	5.9	68.58	68.58
Pressure vessel simulator (PVS)	22.5	68.58	68.58
Void box (VB)*	30.48	68.58	68.58

* Void box dimensions include 0.3175-cm aluminum wall thickness on all sides.

Table 1.2 Material specifications for PCA components outside the core

		Density	Chemical Composition (weight %)								
Material	Type	(g cm^{-3})	Al	P	S	C	Mn	Si	Cr	Ni	Fe
Stainless steel	304L	8.0	-	-	-	≤ 0.03	2.00	1.00	18.00-20.00	8.00-11.00	Balance to 100
Carbon steel	SA-36	7.85	-	0.04	0.05	≤ 0.25					Balance to 100
Aluminum	6061-T6	2.7	100								

Table 1.3 PCA fuel elements

Location*	Element identification	Mass of ^{235}U (grams)	Comments
A-3	A-80	140.131	Standard (18-plate) PCA fuel element
A-4	A-177	140.110	Standard (18-plate) PCA fuel element
A-5	I-116	140.426	Standard (18-plate) PCA fuel element
A-6	B-182	140.230	Standard (18-plate) PCA fuel element
A-7	A-77	140.024	Standard (18-plate) PCA fuel element
B-3	A-55	138.870	Standard (18-plate) PCA fuel element
B-4	B-114	70.640	Safety rod no. 1 (B_4C)
B-5	B-180	140.160	Standard (18-plate) PCA fuel element
B-6	B-127	70.160	Safety rod no. 3 (B_4C)
B-7	A-64	139.200	Standard (18-plate) PCA fuel element
C-3	B-168	140.370	Standard (18-plate) PCA fuel element
C-4	M-49-H	202.000	19-plate ORR fuel element
C-5	B-149-P	132.740	17-plate element**
C-6	M-48-H	202.000	19-plate ORR fuel element
C-7	I-113	140.010	Standard (18-plate) PCA fuel element
D-3	I-115	140.285	Standard (18-plate) PCA fuel element
D-4	B-147	70.070	Safety rod no. 2 (B_4C)
D-5	S-17	140.078	Standard (18-plate) PCA fuel element
D-6	B-197	69.690	Regulating rod (B-SS)
D-7	B-188	140.400	Standard (18-plate) PCA fuel element
E-3	A-81	140.024	Standard (18-plate) PCA fuel element
E-4	A-61	139.070	Standard (18-plate) PCA fuel element
E-5	A-75	139.995	Standard (18-plate) PCA fuel element
E-6	A-60	139.070	Standard (18-plate) PCA fuel element
E-7	I-117	140.257	Standard (18-plate) PCA fuel element
A-2	Auxiliary fission chamber	0.0	Dummy element
E-2	Primary fission chamber	0.0	Dummy element

* See Fig.1.5.

** Plate from the concave side missing. Location of the missing fuel plate used to permit run-to-run monitoring of the core power.

Table 1.4 Selected data on PCA core and fuel elements

PCA CORE	
Total number of MTR plate-type fuel elements	25
Pitch between rows (e.g., A1 to B1 in Fig. 1.2)	8.100 cm (3.189 in.)
Pitch between columns (e.g., A1 to A2 in Fig. 1.2)	7.709 cm (3.035 in.)
STANDARD PCA FUEL ELEMENT (see Fig. 1.6)	
Mass of ^{235}U and enrichment	140 g, 93%
Length	62.548 cm (24.625 in.)
Depth	8.049 cm (3.169 in.)
Width	7.610 cm (2.996 in.)
Number of fuel plates	18
Thickness of water gap between fuel plates	0.297 cm (0.117 in.)
Aluminum side plates (2 per element) (see Fig. 1.7)* Thickness Width	 ~ 0.338 cm (~ 0.133 in.) 8.049 cm (3.169 in.)
HOMOGENIZED FUELED REGION OF THE STANDARD FUEL ELEMENT	
Volume Volume of aluminum Volume of water	3747 cm^3 8.10 × 7.71 × 60.008 cm^3 (3.189 in. × 3.035 in. × 23.625 in.) ~ 1515.9 cm^3 ~ 2231.1 cm^3
STANDARD PCA FUEL ELEMENT FUEL PLATE (see Fig. 1.8)	
Plate width before bending	7.226 cm (2.845 in.)
Length of fueled region in plate	60.008 cm (23.625 in.)
Width of the fueled region in plate	6.350 cm (2.5 in.)
Total plate thickness Layers of Al cladding (2 layers) Fueled region (Al-U alloy)	0.152 cm (0.060 in.) 0.051 cm (0.020 in.) each 0.051 cm (0.020 in.)

Table 1.4 (continued)

CONTROL ROD ELEMENT (see Fig. 1.9)	
Mass of ^{235}U and enrichment	70 g, 93%
Number of fuel plates	9
Width of control rod guide	6.655 cm (2.62 in.)
Depth of control rod guide	2.858 cm (1.125 in.)
SPECIFICATIONS FOR M-48-H AND M-49-H FUEL ELEMENTS	
Mass of ^{235}U and enrichment	200 g, 93%
Length	62.548 cm (24.625 in.)
Depth	8.049 cm (3.169 in.)
Width	7.610 cm (2.996 in.)
Thickness of water gap between fuel plates	0.295 cm (0.116 in.)
Number of fuel plates	19
Length of fueled region in plate	60.008 cm (23.625 in.)
Width of fueled region in plate	6.350 cm (2.5 in.)
Thickness of fueled region in plate	0.051 cm (0.02 in.)
Cladding thickness (inside plate)	0.038 cm (0.015 in.)
Cladding thickness (end plate)	0.057 cm (0.0225 in.)

* Aluminum side plates have a relatively complicated geometry. The thickness of the plate in the fueled region was estimated from drawing D-7207 as the average of 0.198 cm (0.078 in.) and 0.478 cm (0.188 in.). The width of the plate was obtained from the same drawing.

Table 1.5 Horizontal relative power density distribution*

COORDINATE X \ Y → ↓		COLUMN 5			COLUMN 6			COLUMN 7		
	(cm)	**-2.34**	**0.00**	**2.34**	**5.37**	**7.71**	**10.05**	**13.08**	**15.42**	**17.76**
ROW	**1.15**	1.68	1.62	1.68	1.60	1.48	1.43	1.30	1.13	1.16
A	**4.30**	1.80	1.79	1.80	1.73	1.63	1.55	1.36	1.23	1.31
	7.45	2.23	2.13	2.23	2.23	2.06	1.95	1.73	1.43	1.55
ROW	**9.25**	2.54	2.33	2.54	2.87	2.72	2.51	1.98	1.60	1.75
B	**12.40**	2.96	2.67	2.96	0.00	0.00	0.00	2.25	1.82	1.98
	15.55	2.88	2.76	2.88	2.82	2.66	2.43	2.18	1.87	1.98
ROW	**17.35**	2.82	2.87	2.82	3.55	3.37	3.17	2.19	1.99	2.13
C	**20.50**	2.79	2.83	2.79	3.43	3.08	3.08	2.19	1.96	2.09
	23.65	2.82	2.78	2.82	3.75	3.43	3.29	2.23	2.00	2.06

* Coordinates are given in coordinate system defined on Fig. 1.10. Relative power densities $p(x_i,y_i)$ are multiplied by 100. The rows (A to C) and columns (5 to 7) of the fuel elements are labeled as in the Figs. 1.2 and 1.5.

Table 1.6 Experimental results for fission chamber and radiometric measurements of equivalent fission fluxes

Location	Distance* (cm)	Equivalent fission fluxes** [per 1 PCA core fission neutron per second (cm^{-2})]					
		^{237}Np	^{238}U	^{103}Rh	^{115}In	^{58}Ni	^{27}Al
A1	12.0	6.64 E-6 ± 6.2%	-	5.54 E-6 ± 1.0%	5.61 E-6 ± 1.0%	5.83 E-6 ± 1.4%	7.87 E-6 ± 1.0%
A2	23.8	-	-	-	6.06 E-7 ± 2.0%	6.18 E-7 ± 2.0%	1.02 E-6 ± 2.0%
A3	29.7	2.27 E-7 ± 6.3%	-	-	1.99 E-7 ± 1.0%	2.31 E-7 ± 1.4%	4.48 E-7 ± 1.0%
A4	39.5	9.27 E-8 ± 5.5%	6.11 E-8 ± 6.9%	7.74 E-8 ± 1.5%	5.87 E-8 ± 0.7%	5.30 E-8 ± 1.0%	1.02 E-7 ± 2.0%
A5	44.7	5.18 E-8 ± 5.7%	2.74 E-8 ± 6.8%	4.35 E-8 ± 5.0%	2.76 E-8 ± 1.5%	2.09 E-8 ± 1.8%	4.10 E-8 ± 2.2%
A6	50.1	2.70 E-8 ± 5.8%	1.12 E-8 ± 7.1%	2.19 E-8 ± 5.0%	1.17 E-8 ± 3.0%	7.43 E-9 ± 2.2%	1.54 E-8 ± 2.2%
A7	59.1	7.25 E-9 ± 9.2%	-	-	-	-	-
Reaction cross sections, averaged over ^{235}U fission spectrum * (mb)**							
		1312 ± 50	305 ± 9	733 ± 38	189 ± 8	109 ± 6	0.705 ± 0.040

* Distance to core face of the aluminum window.

** For the ^{237}Np and ^{238}U equivalent fission fluxes, the combined uncertainties are given. For all others, the experimental precision only is given. (The experimental precision, as defined in Ref. 1, encompasses foil size corrections, if any; counting statistics; dead time; pileup and background corrections; corrections for interfering reactions; run-to-run monitoring; and positional uncertainties in a given experimental channel.) The combined uncertainties for ^{103}Rh, ^{115}In, ^{58}Ni, and ^{27}Al equivalent fission fluxes are ± 6%, for a precision of 1%.

*** Cross sections and their absolute standard deviations are from Ref. 1.

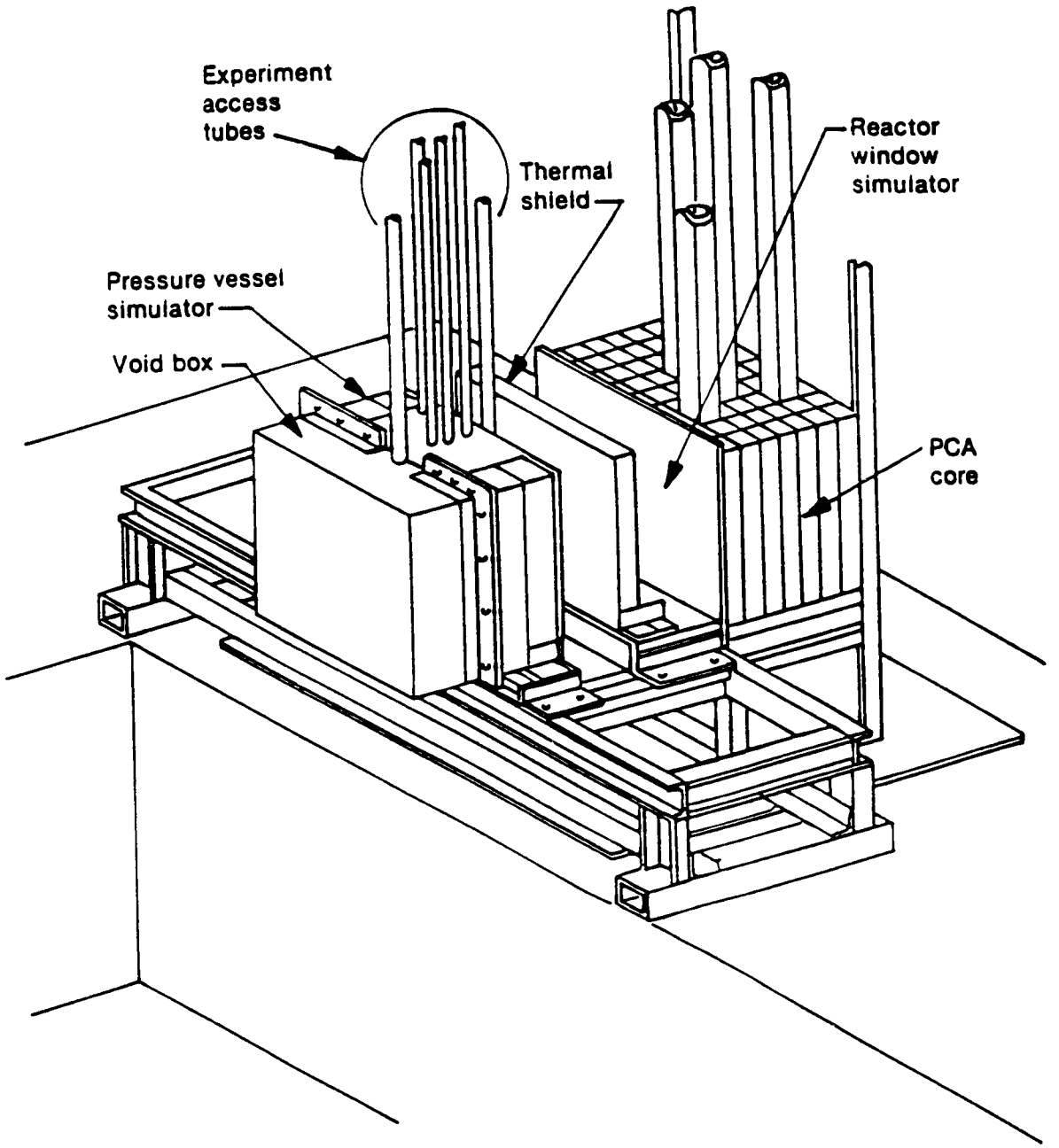

Fig. 1.1 PCA pressure vessel wall benchmark facility

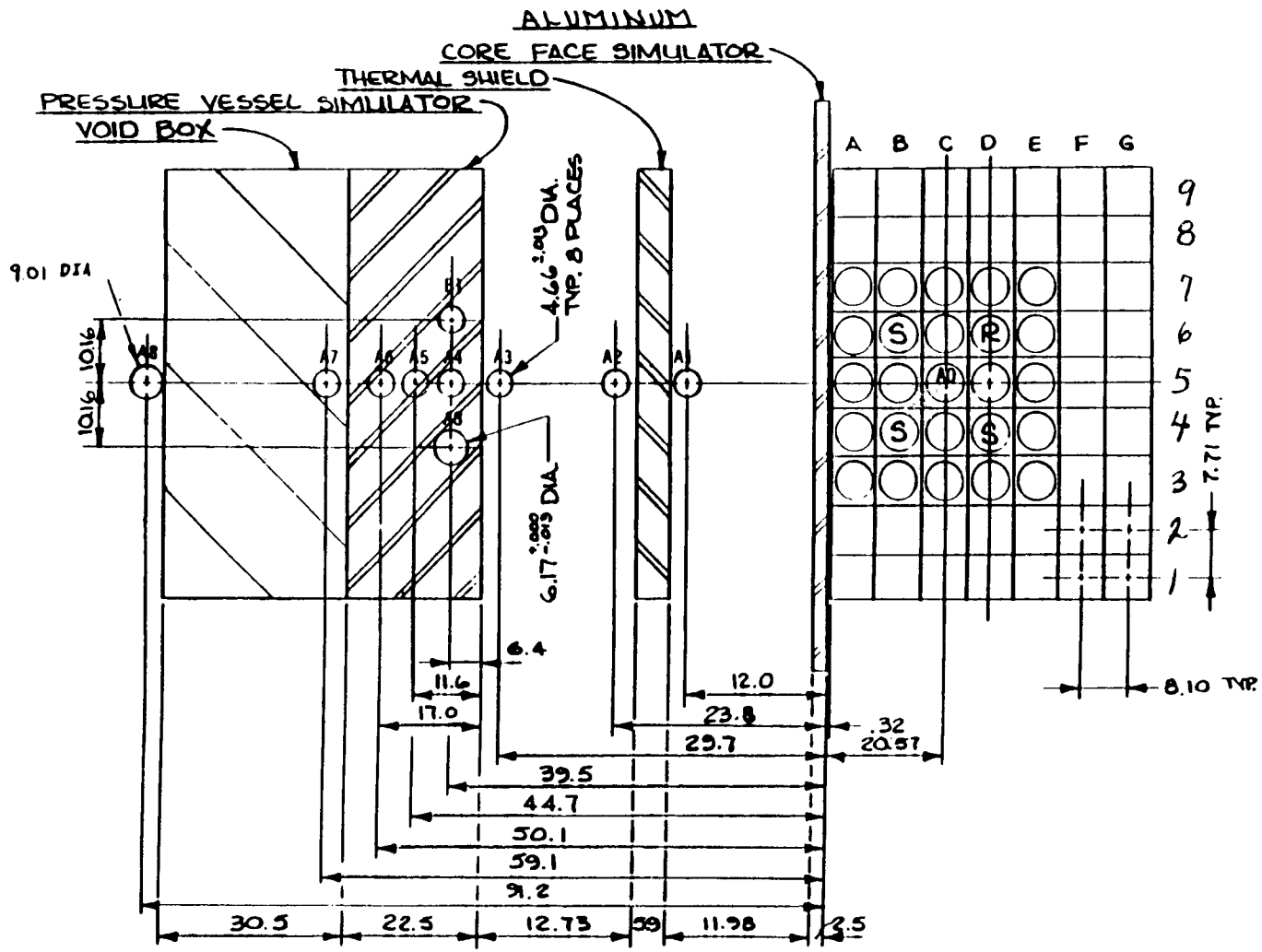

Fig. 1.2 Horizontal cross section of the PCA pressure vessel benchmark facility 12/13 configuration
(dimensions are in cm)

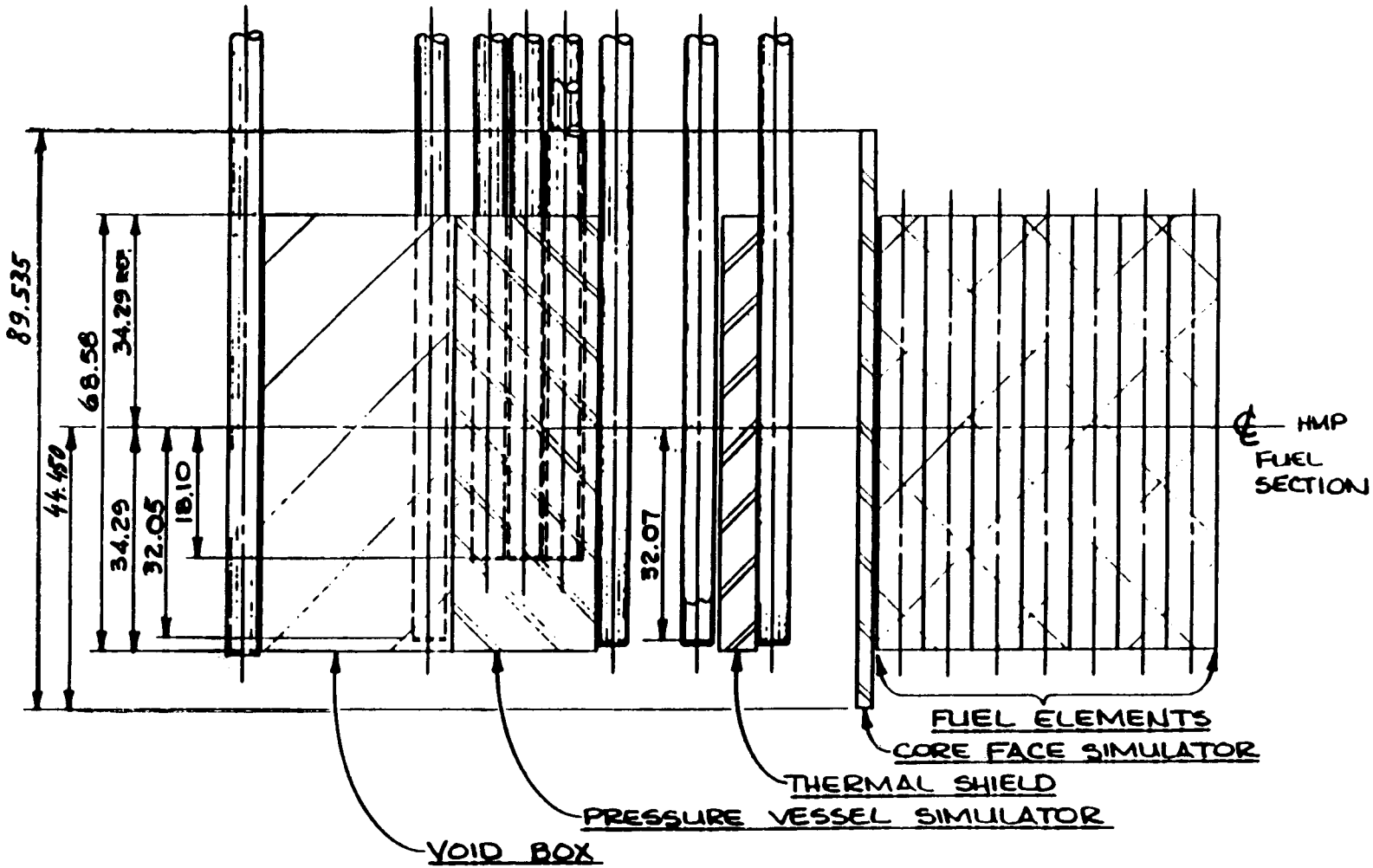

Fig. 1.3 Vertical cross section of the PCA pressure vessel benchmark facility (dimensions are in cm)

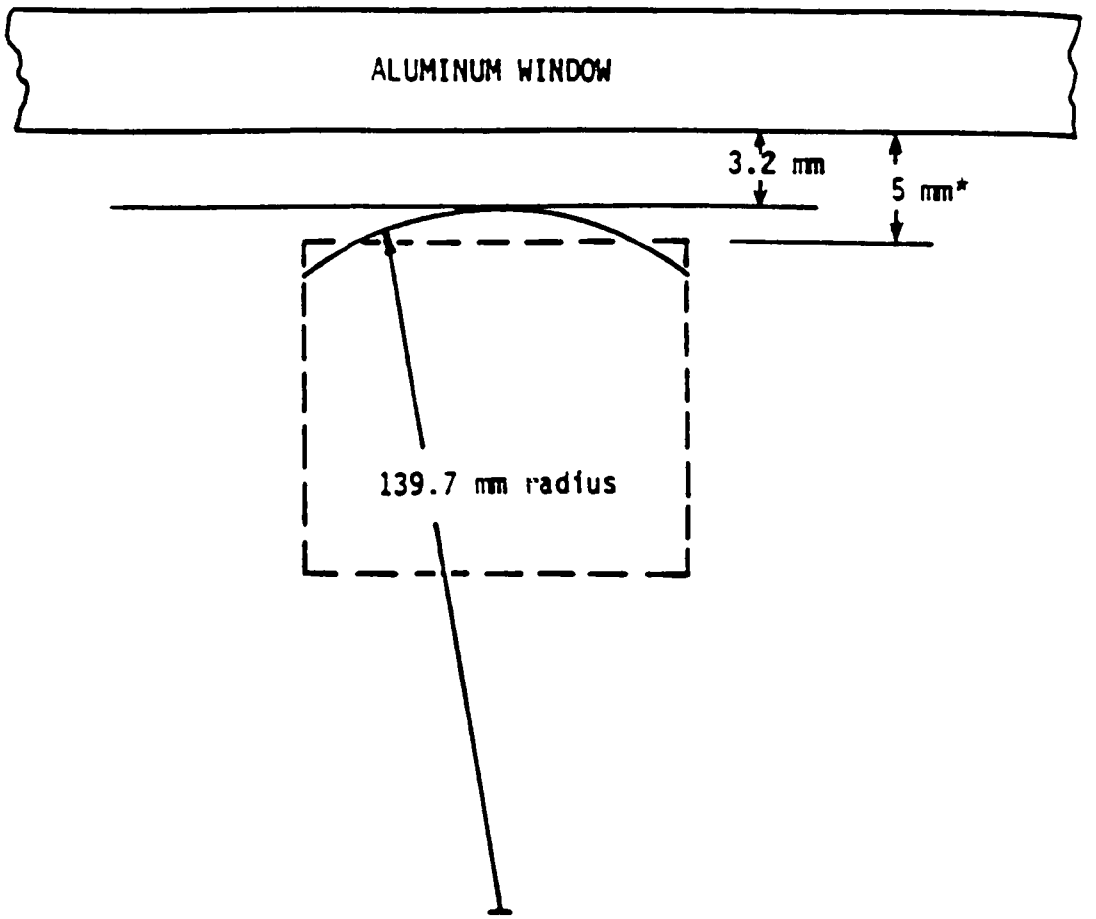

*1.8 mm accounts for fuel plate curvature

Fig. 1.4 Detail of the interface of the PCA fuel cell boundary and the core aluminum window. The MTR plate-type fuel element has curved fuel plates. The physical gap between the aluminum window and the closest surface area of the curved fuel plates is 3.2 mm, as shown in Fig. 1.2. If, however, the fuel element cross section is modeled as a rectangle, than the centroid through the last fuel plate is 5 mm from the aluminum window, as shown above.

	1	2	3	4	5	6	7	8	9
A		AUX FC	140 A-80	140 A-177	140 I-116	140 B-182	140 A-77		
B			140 A-55	S-1 70 B-114	140 B-180	S-3 70 B-127	140 A-64		
C			140 B-168	200 M-49-H	133 B-149-P	200 M-48-H	140 I-113		
D			140 I-115	S-2 70 B-147	140 S-17	RR 70 B-197	140 B-188		
E		PRI FC	140 A-81	140 A-61	140 A-75	140 A-60	140 I-117		
F									
G									

Critical Rod Positions: No. 1 Safety .....48.26 cm (19.0 in.)
No. 2 Safety.....48.26 cm (19.0 in.)
No. 3 Safety.....48.26 cm (19.0 in.)
Regulating Rod.....38.43 cm (15.13 in.)

Critical mass of ^{235}U..... 3336.01 g

Fig. 1.5 Fuel loading pattern for the PCA pressure vessel experiment. For each fuel element in the PCA core the approximate (within 1%) mass of ^{235}U in grams (top number) and the element identification are given. Safety rods 1-3 are denoted by S-1, S-2, and S-3. The regulating rod is denoted by RR. Note that the fuel elements are not precisely square and that there is a water gap between each element. The pitch between rows (e.g., A to B) is 8.10 cm (3.189 in.) and the pitch between columns is 7.709 cm (3.035 in.). See Table 1.4 for details on the PCA core and fuel elements.

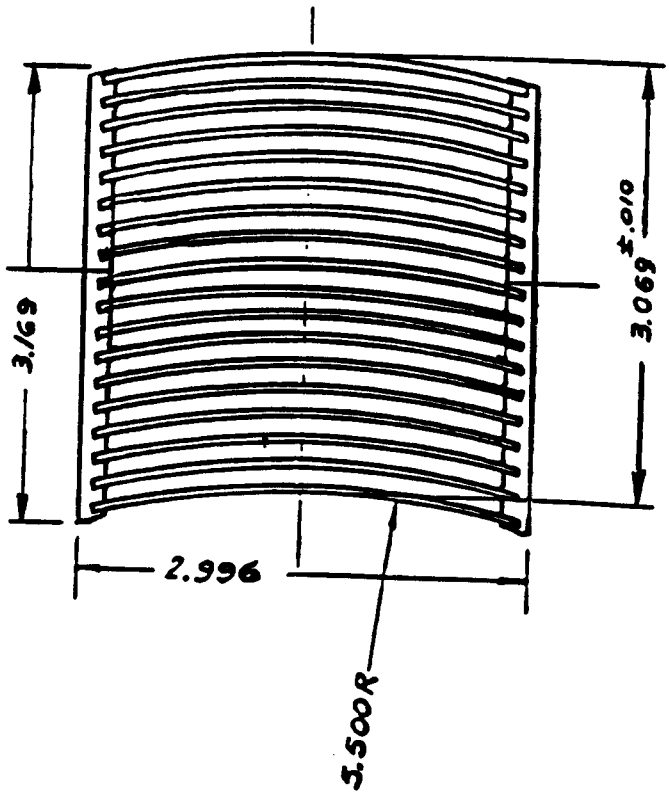

Fig. 1.6 Cross section of the standard PCA fuel element with 18 fuel plates
(dimensions in inches)

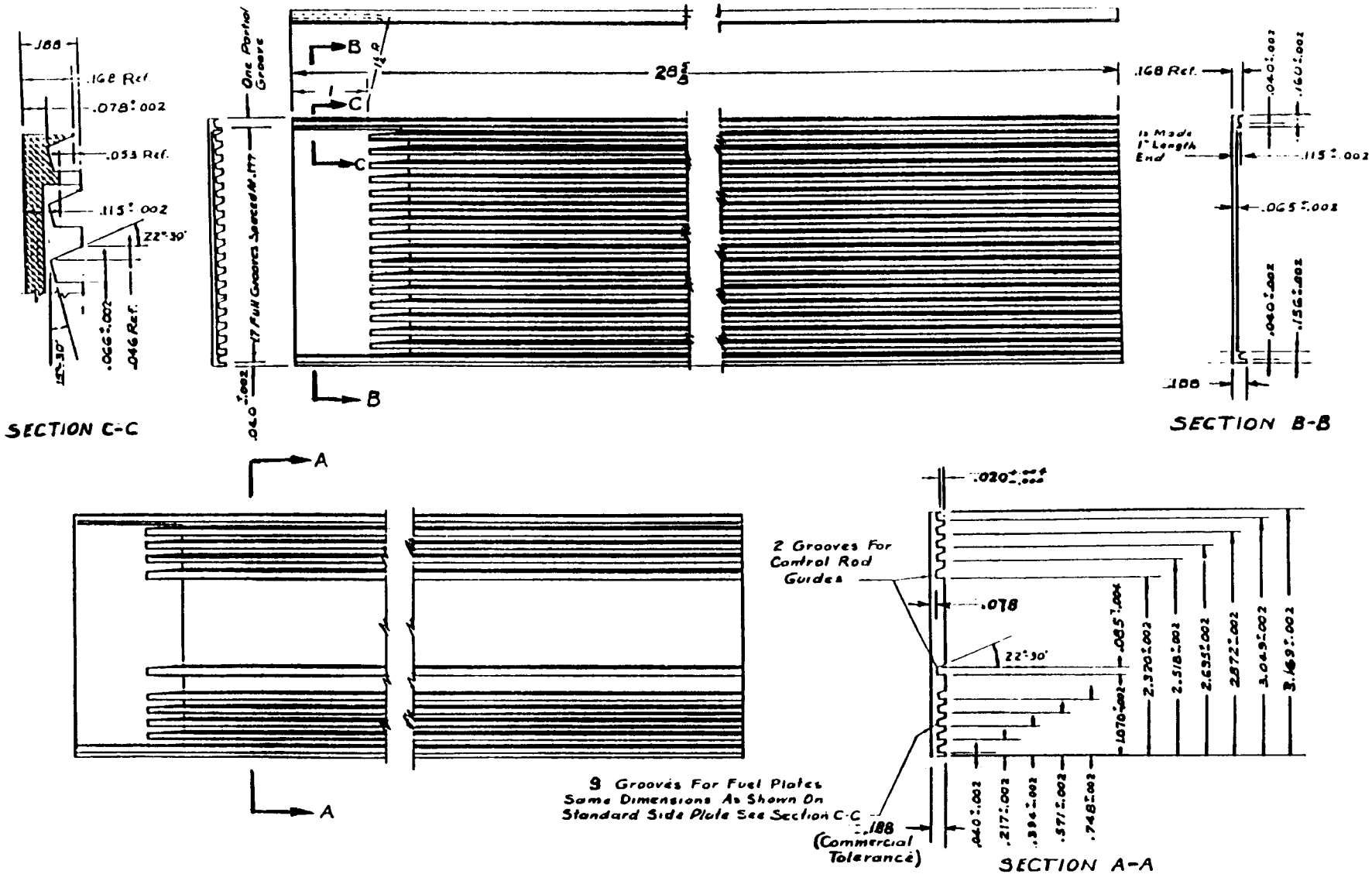

Fig 1.7 Depiction of the aluminum side plates, taken from drawing D-7207 ("Fuel & Side Plates"), for the standard fuel element (*top*) and control-rod fuel element (*bottom*) (all dimensions in inches)

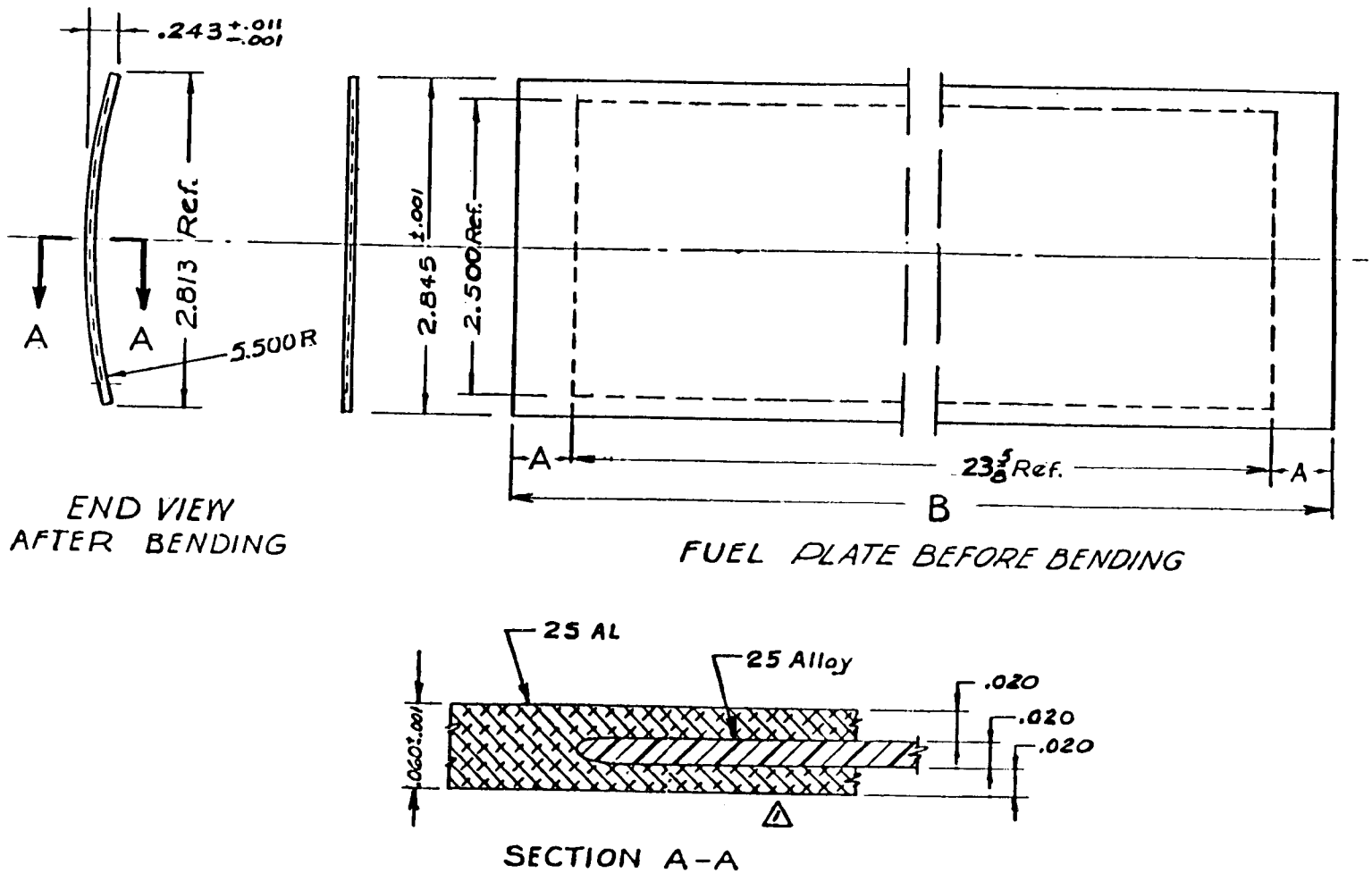

Fig. 1.8 Details of the standard fuel plate, taken from drawing D-7207 ("Fuel & Side Plates")
(all dimensions in inches)

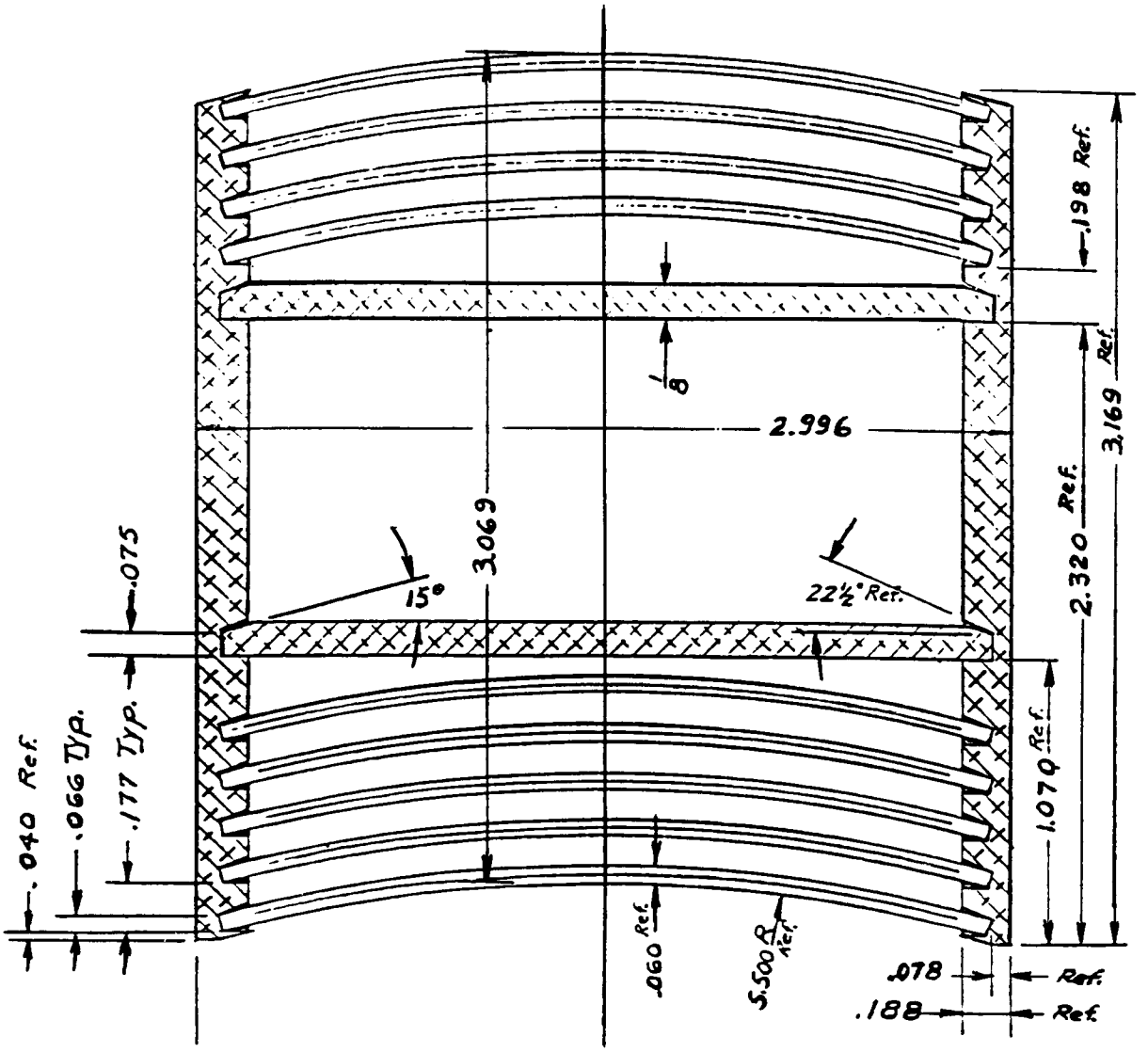

Fig. 1.9 Horizontal cross section (through the fueled region) of the control-rod fuel element, taken from drawing D-7206 ("Special Fuel Element for Control Rod")
(all dimensions in inches)

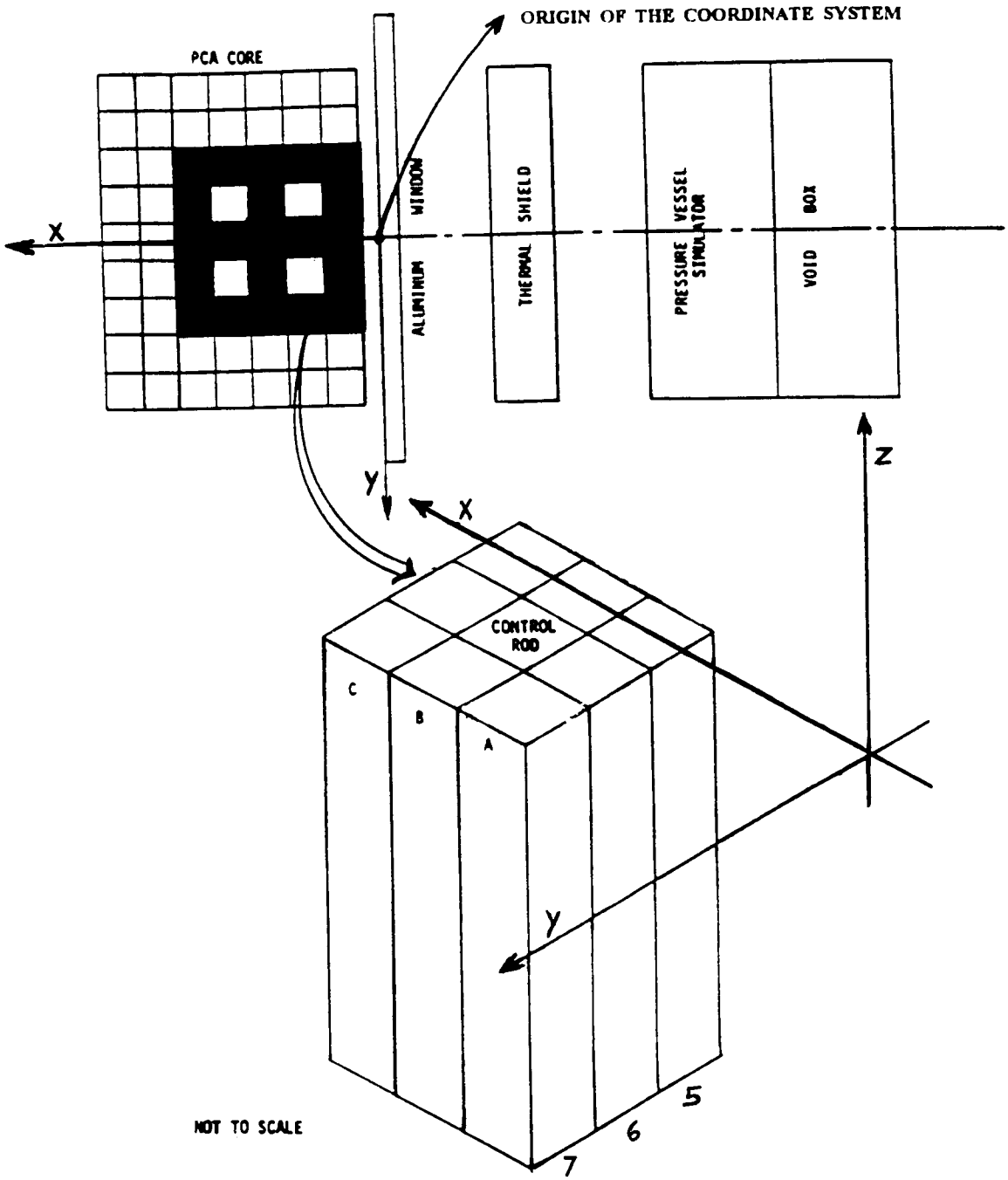

Fig 1.10 Coordinate system used for description of PCA core power distribution

A5 0.94224	A6 0.86627	A7 0.66450
B5 1.3781	B6 0.30493 Control rod 0.49147	B7 0.95617
C5 1.4707	C6 1.6739	C7 1.0388
D5 1.3959	D6 0.35159 Control rod 0.44434	D7 0.96602
E5 1.0231	E6 0.93036	E7 0.70665

Fig 1.11 Relative fuel element powers. Normalization is to the core average fuel element power of 1.000. The core is symmetric across the *X*-axis (that is, across the center line through elements A5 to E5). For the elements with control rods (B6 and D6) relative power is given for each of the two fueled sections. See also Figs. 1.6-1.9 for the details of the fuel elements and control rods.

2 BENCHMARK ANALYSIS

2.1 METHODOLOGY

The transport calculations were performed using the DORT,[1] computer code (Ref. 1) which is based on the method of discrete ordinates. Three calculations were performed: one *x-y*, one *z-x*, and a one-dimensional *x*-calculation. The flux synthesis method was then used to obtain the fluxes at the desired locations. The flux synthesis method, described in more detail in Ref. 2, combines two- and one-dimensional transport calculations to obtain an estimation of the neutron fluxes in the three-dimensional geometries. For the flux synthesis the DOTSYN code (Ref. 3) was used.

The transport calculations were done in Cartesian coordinates. The horizontal cross section of the facility was modeled in the *x-y* calculation. The geometry model took advantage of the quarter core symmetry, and only one quadrant of the core was modeled. The model covered part of the geometry shown in Fig 1.2, extending in the *x*-direction from the center line of the fuel elements in the row C to the water region behind the void box, and in the *y* direction, from the center line of the fuel elements in the column 5 to the inside of the water region at the core side. There were 140 and 59 mesh intervals used in the *x*- and *y*-directions, respectively. Each fuel element was described by an array of 9 by 6 mesh intervals in the *x*- and *y*-direction, respectively. The *z-x* geometry model, which described the vertical cross-section of the facility, used the same *x*-mesh as the *x-y* model. In the vertical (*z*) direction the model extended from 25 cm below the core to 25 cm above the core. Of 73 *z*-intervals, 39 equal-width intervals were used to cover the height of active fuel. The one-dimensional (*x*) calculation used the same *x*-mesh as the *x-y* and *z-x* calculations.

The flux synthesis method requires that the neutron sources for the three calculations are prepared in a consistent manner: the sources for the *x-y*, *z-x*, and *x* calculations are obtained by integrating the spatial source distribution over the *z*, *y*, and both *z* and *y* coordinates, respectively. Therefore, from the PCA core-power distribution given in Eq. (1.1), and the data from Fig. 1.11 and Table 1.5 of this report, the sources were prepared as follows. For the neutron source distribution in the *x-y* calculation, the "point" values from Table 1.5 were renormalized to give the fuel-element relative powers listed in Fig. 1.11,[2] and then used to approximate the averages over one-ninth of the fuel-element cross section. The source distribution for the *z-x* calculation was described as a product of the distributions in the *x*-direction and in the vertical (*z*-) direction. The distribution in the *x*-direction was obtained by integrating the source for the *x-y* calculation over the *y* coordinate (from

---

[1]DORT version 2.12.14, dated 14 December 1994, was used.

[2]For the element at location B6, which contains the control rod, weights of 2/27 and 1/9 of the fuel-element cross section were used for the points closer to the aluminum window and further from the aluminum window, respectively, in order to approximate different volumes of the fueled regions on each side of the control rod area.

the center line to the edge of the core). The source distribution in the z-direction was generated from the cosine distribution given in Eq. 1.1 which was normalized to provide the integral of 1.00 when integrated over the height of the core. For the one-dimensional (x) calculation, the source distribution in the x-direction from the z-x calculation was used. The fuel in the PCA core was fresh, highly enriched uranium; therefore, the ENDF/B-VI fission spectrum of the ^{235}U was used for the source spectrum.

The core region was homogenized using data for the standard fuel element (see Table 1.4). The geometrical regions outside the core coincided with the material regions (water, aluminum, stainless steel, or carbon steel). The P_3 approximation to the angular dependence of the anisotropic scattering cross sections (e.g., the P_0 to P_3 Legendre components) and the symmetric S_8 "directional quadrature set" (e.g., the set of discrete directions and angular quadratures) were used for all transport calculations. The macroscopic cross sections were prepared by the GIP code (Ref. 4). The cross sections for the transport calculations were taken from three ENDF/B-VI-based libraries: BUGLE-93 (Ref. 5), SAILOR-95[3], and BUGLE-96 (Ref. 6). These three libraries have the same energy group structure with 47 neutron groups. The PCA analysis was performed separately with each of these libraries.

The neutron spectra, normalized to the neutron source in the PCA core of one neutron per second, were synthesized for all dosimetry locations. Reaction rates were calculated with dosimetry cross sections from CROSS-95 (Ref. 7). The reaction rates were converted to the equivalent fission fluxes using the cross sections averaged over the ^{235}U fission spectrum, which are given in Table 1.6.

[3]M. L. Williams, M. Asgari, and H. Manohara, Letter Report on Generating SAILOR-95 Library, personal communication, February 1995.

2.2 RESULTS AND DISCUSSION

The reaction rates at the dosimetry locations were determined with the group fluxes from the transport calculations. The same dosimetry cross sections, taken from CROSS-95 (Ref. 7), were used with the group fluxes from the calculations with the BUGLE-93, SAILOR-95 and BUGLE-96 libraries.[4] The reaction rates are compared in Table 2.1. Only the reactions for which the measurements were done are listed. The reaction rates predicted with the three ENDF/B-VI- based libraries for transport calculations are in good agreement. In particular, all compared reaction rates obtained with BUGLE-96 and SAILOR-95 agree to within 2.2% at all dosimetry locations. BUGLE-96 reaction rates are slightly lower, from ~1% to ~2.2%, than SAILOR-95. The only exception is the highest threshold reaction, ^{27}Al(n,α), for which BUGLE-96 calculations predicted reaction rates 1.0% to 2.0% higher than did SAILOR-95. The results with BUGLE-93 agree well, to within ~2%, with the other two libraries for the ^{27}Al(n,α), ^{58}Ni(n,p), ^{103}Rh(n,n') and ^{115}In(n,n') reactions at the locations A1 to A6—that is, from the position in front of the thermal shield to the 3/4 thickness of the pressure vessel. In the void box behind the pressure vessel (A7) and in the water behind the void box (A8) the differences between BUGLE-93 and other two libraries were up to ~6%, with BUGLE-93 reaction rates being lower. This appears to be a consequence of different self-shielding of the steel cross-section used in the libraries (Ref. 8). The BUGLE-93 predictions for the ^{237}Np(n,f) reaction rates show big differences from the other two libraries at the locations in the water (i.e., locations A1, A2, A3, and A8), and smaller, but still important, differences in the air-filled box behind the thermal shield (location A7). These differences were caused by the known deficiencies in the BUGLE-93 thermal cross sections (Ref. 8), which cause an overprediction of the thermal flux. These deficiencies also affected the ^{238}U(n,f) reaction rates, but to a much smaller degree. When the ^{237}Np(n,f) reaction rates are calculated without the contribution from thermal neutrons (below 0.41 eV), the BUGLE-93 results are in good agreement, similar to those for the other reactions, with the other two libraries (see Table 2.1). Therefore, the BUGLE-93 library should not be used for calculating the reaction rates of thermal neutron reactions in any environment, nor for any reaction rates with a nonzero contribution from thermal neutrons in the water environments.

---

[4]The cross sections in the CROSS-95 library are in 640 groups. They were collapsed to the 47 groups with the code FLXPRO using the 640 groups reference spectrum (consisting of the Watt fission spectrum matched to 1/E spectrum at 0.5 MeV and to the Maxwellian thermal spectrum with neutron temperature 323.16 K at 0.14 eV), and the calculated spectrum from the location A4 in the PCA pressure vessel simulator. The effects of the different dosimetry cross sections and collapsing procedures are discussed in Appendix A. On FLXPRO, see F.W. Stallman, *LSL-M2: A Computer Program for Least-Square Logarithmic Adjustment of Neutron Spectra*, NUREG/CR-4349 (ORNL/TM-9933), March 1996.

Table 2.1 Comparison of the reaction rates obtained from the calculations with BUGLE-93, SAILOR-95, and BUGLE-96 cross sections for transport calculations

LOCATION	A BUGLE-93 ($s^{-1}atom^{-1}$)	DIFF. (A-B)/B (%)	B SAILOR-95 ($s^{-1}atom^{-1}$)	DIFF. (C-B)/B (%)	C BUGLE-96 ($s^{-1}atom^{-1}$)
A1					
$^{27}Al(n,\alpha)$	5.18E-33	0.0	5.18E-33	1.0	5.23E-33
$^{58}Ni(n,p)$	5.84E-31	0.0	5.84E-31	-2.0	5.72E-31
$^{103}Rh(n,n')$	3.88E-30	0.3	3.87E-30	-2.0	3.79E-30
$^{115}In(n,n')$	9.84E-31	0.2	9.82E-31	-2.2	9.60E-31
$^{238}U(n,f)$	1.66E-30	2.1	1.62E-30	-2.2	1.59E-30
$^{237}Np(n,f)$	2.14E-29	171.6	7.89E-30	-1.9	7.74E-30
$^{238}U(n,f)$*	1.62E-30	0.1	1.62E-30	-2.2	1.59E-30
$^{237}Np(n,f)$*	7.43E-30	0.3	7.41E-30	-1.9	7.27E-30
A2					
$^{27}Al(n,\alpha)$	6.62E-34	0.0	6.62E-34	1.2	6.70E-34
$^{58}Ni(n,p)$	6.21E-32	-0.0	6.21E-32	-1.7	6.10E-32
$^{103}Rh(n,n')$	4.41E-31	0.0	4.41E-31	-1.9	4.33E-31
$^{115}In(n,n')$	1.07E-31	0.0	1.06E-31	-2.0	1.04E-31
$^{238}U(n,f)$	1.77E-31	1.4	1.75E-31	-2.0	1.71E-31
$^{237}Np(n,f)$	1.95E-30	111.3	9.25E-31	-1.9	9.08E-31
$^{238}U(n,f)$*	1.75E-31	-0.1	1.75E-31	-2.0	1.71E-31
$^{237}Np(n,f)$*	8.66E-31	0.0	8.65E-31	-1.9	8.49E-31
A3					
$^{27}Al(n,\alpha)$	3.04E-34	0.0	3.04E-34	1.3	3.08E-34
$^{58}Ni(n,p)$	2.38E-32	0.0	2.38E-32	-1.5	2.35E-32
$^{103}Rh(n,n')$	1.44E-31	0.2	1.44E-31	-1.8	1.41E-31
$^{115}In(n,n')$	3.66E-32	0.1	3.65E-32	-1.9	3.59E-32
$^{238}U(n,f)$	6.30E-32	2.0	6.17E-32	-1.8	6.06E-32
$^{237}Np(n,f)$	7.90E-31	169.7	2.93E-31	-1.8	2.88E-31
$^{238}U(n,f)$*	6.17E-32	-0.0	6.17E-32	-1.8	6.05E-32
$^{237}Np(n,f)$*	2.75E-31	0.2	2.75E-31	-1.8	2.70E-31
A4					
$^{27}Al(n,\alpha)$	6.84E-35	0.0	6.84E-35	1.4	6.93E-35
$^{58}Ni(n,p)$	5.34E-33	-0.1	5.34E-33	-1.4	5.27E-33
$^{103}Rh(n,n')$	5.57E-32	0.3	5.56E-32	-1.8	5.46E-32
$^{115}In(n,n')$	1.09E-32	-0.2	1.10E-32	-1.8	1.08E-32
$^{238}U(n,f)$	1.69E-32	-0.3	1.70E-32	-1.8	1.67E-32
$^{237}Np(n,f)$	1.16E-31	1.1	1.15E-31	-1.8	1.13E-31
$^{238}U(n,f)$*	1.69E-32	-0.3	1.70E-32	-1.8	1.67E-32
$^{237}Np(n,f)$*	1.15E-31	0.1	1.15E-31	-1.8	1.13E-31

Table 2.1 (continued)

LOCATION	A BUGLE-93 ($s^{-1}atom^{-1}$)	DIFF. (A-B)/B %	B SAILOR-95 ($s^{-1}atom^{-1}$)	DIFF. (C-B)/B %	C BUGLE-96 ($s^{-1}atom^{-1}$)
A5					
$^{27}Al(n,\alpha)$	2.71E-35	0.0	2.71E-35	1.5	2.75E-35
$^{58}Ni(n,p)$	2.08E-33	-0.3	2.09E-33	-1.4	2.06E-33
$^{103}Rh(n,n')$	2.98E-32	-0.2	2.99E-32	-1.8	2.93E-32
$^{115}In(n,n')$	4.96E-33	-0.8	5.00E-33	-1.8	4.91E-33
$^{238}U(n,f)$	7.24E-33	-0.8	7.30E-33	-1.7	7.17E-33
$^{237}Np(n,f)$	6.30E-32	-0.6	6.33E-32	-1.8	6.22E-32
$^{238}U(n,f)$*	7.24E-33	-0.8	7.30E-33	-1.7	7.17E-33
$^{237}Np(n,f)$*	6.29E-32	-0.6	6.33E-32	-1.8	6.22E-32
A6					
$^{27}Al(n,\alpha)$	1.02E-35	0.0	1.02E-35	1.6	1.03E-35
$^{58}Ni(n,p)$	7.64E-34	-0.5	7.68E-34	-1.3	7.57E-34
$^{103}Rh(n,n')$	1.46E-32	-1.5	1.49E-32	-1.8	1.46E-32
$^{115}In(n,n')$	2.09E-33	-1.8	2.13E-33	-1.8	2.09E-33
$^{238}U(n,f)$	2.88E-33	-1.4	2.92E-33	-1.7	2.87E-33
$^{237}Np(n,f)$	3.14E-32	-2.0	3.21E-32	-1.8	3.15E-32
$^{238}U(n,f)$*	2.88E-33	-1.4	2.92E-33	-1.7	2.87E-33
$^{237}Np(n,f)$*	3.14E-32	-2.1	3.21E-32	-1.8	3.15E-32
A7					
$^{27}Al(n,\alpha)$	3.10E-36	0.0	3.10E-36	1.7	3.15E-36
$^{58}Ni(n,p)$	1.95E-34	-0.9	1.97E-34	-1.3	1.94E-34
$^{103}Rh(n,n')$	3.69E-33	-6.0	3.92E-33	-1.8	3.85E-33
$^{115}In(n,n')$	5.22E-34	-3.9	5.43E-34	-1.8	5.33E-34
$^{238}U(n,f)$	7.17E-34	-2.0	7.31E-34	-1.7	7.19E-34
$^{237}Np(n,f)$	9.81E-33	13.1	8.67E-33	-1.9	8.51E-33
$^{238}U(n,f)$*	7.12E-34	-2.6	7.31E-34	-1.7	7.18E-34
$^{237}Np(n,f)$*	8.00E-33	-6.4	8.55E-33	-1.9	8.39E-33
A 8					
$^{27}Al(n,\alpha)$	8.20E-37	0.0	8.19E-37	2.0	8.36E-37
$^{58}Ni(n,p)$	4.34E-35	-0.5	4.36E-35	-1.0	4.31E-35
$^{103}Rh(n,n')$	4.04E-34	-3.7	4.20E-34	-1.5	4.14E-34
$^{115}In(n,n')$	7.80E-35	-2.1	7.96E-35	-1.4	7.85E-35
$^{238}U(n,f)$	1.33E-34	5.0	1.27E-34	-1.4	1.25E-34
$^{237}Np(n,f)$	4.35E-33	311.1	1.06E-33	-1.5	1.04E-33
$^{238}U(n,f)$*	1.24E-34	-1.6	1.26E-34	-1.4	1.24E-34
$^{237}Np(n,f)$*	8.62E-34	-4.1	8.98E-34	-1.5	8.85E-34

* Reaction rates were calculated without the contribution from the two thermal groups below 0.41 eV. Data for these groups are incorrect for BUGLE-93.

The equivalent fission fluxes were calculated by dividing the reaction rates by the cross sections averaged over the ^{235}U fission spectrum, taken from Table 1.6. The ratios of the calculated-to-measured (C/M) equivalent fission fluxes for BUGLE-93, SAILOR-95, and BUGLE-96 are given in Tables 2.2, 2.3 and 2.4. An excellent agreement of the calculations with the measurements has been obtained. The average C/M ratio for all the measurements (a total of 31) was 0.92 ± 0.03 for the BUGLE-96 library and 0.93 ± 0.03 for the SAILOR-95 library. For the BUGLE-93 library the average C/M ratio for all dosimeters (a total of 28), except the ^{237}Np at locations in water (A1 and A3) and in the air-filled box behind the pressure vessel (A7), was 0.93 ± 0.03.

Table 2.2 Ratios of calculated-to-measured (C/M) equivalent fission fluxes obtained by the BUGLE-93 library

Location*	$^{237}Np(n,f)$**	$^{238}U(n,f)$	$^{27}Al(n,\alpha)$	$^{58}Ni(n,p)$	$^{115}In(n,n')$	$^{103}Rh(n,n')$	Av. ± std.
A1	2.46 (0.85)	-	0.93	0.92	0.93	0.95	0.93 ±0.01***
A2	-	-	0.92	0.92	0.93	-	0.92 ±0.01
A3	2.65 (0.92)	-	0.96	0.95	0.97	-	0.96 ±0.01***
A4	0.96 (0.95)	0.91	0.95	0.92	0.99	0.98	0.95 ±0.03
A5	0.93 (0.93)	0.87	0.94	0.91	0.95	0.93	0.92 ±0.03
A6	0.89 (0.89)	0.84	0.94	0.94	0.95	0.91	0.91 ±0.04
A7	1.03 (0.84)	-	-	-	-	-	-

* Locations are shown in Fig. 1.2.

** The C/M for $^{237}Np(n,f)$, which are given in parentheses, were calculated with the reaction rates for the spectrum above 0.41 eV—that is, excluding the two thermal groups. The C/M without parentheses are for reaction rates for the full spectrum.

*** Average without the C/M for $^{237}Np(n,f)$.

Table 2.3 Ratios of calculated-to-measured (C/M) equivalent fission fluxes obtained by the SAILOR-95 library

Location*	^{237}Np(n,f)	^{238}U(n,f)	^{27}Al(n,α)	^{58}Ni(n,p)	^{115}In(n,n')	^{103}Rh(n,n')	Av. ± std.
A1	0.91	-	0.93	0.92	0.93	0.95	0.93 ±0.01
A2	-	-	0.92	0.92	0.93	-	0.92 ±0.01
A3	0.98	-	0.96	0.95	0.97	-	0.97 ±0.01
A4	0.94	0.91	0.95	0.92	0.99	0.98	0.95 ±0.03
A5	0.93	0.87	0.94	0.92	0.96	0.94	0.93 ±0.03
A6	0.91	0.85	0.94	0.95	0.96	0.93	0.92 ±0.04
A7	0.91	-	-	-	-	-	0.91

* Locations are shown in Fig. 1.2.

Table 2.4 Ratios of calculated-to-measured (C/M) equivalent fission fluxes obtained by the BUGLE-96 library

Location*	^{237}Np(n,f)	^{238}U(n,f)	^{27}Al(n,α)	^{58}Ni(n,p)	^{115}In(n,n')	^{103}Rh(n,n')	Av. ± std.
A1	0.89	-	0.94	0.90	0.91	0.93	0.91 ±0.02
A2	-	-	0.93	0.91	0.91	-	0.92 ±0.01
A3	0.97	-	0.98	0.93	0.95	-	0.96 ±0.02
A4	0.93	0.90	0.96	0.91	0.97	0.96	0.94 ±0.03
A5	0.92	0.86	0.95	0.90	0.94	0.92	0.92 ±0.03
A6	0.89	0.84	0.95	0.94	0.95	0.91	0.91 ±0.04
A7	0.89	-	-	-	-	-	0.89

* Locations are shown in Fig. 1.2.

The average C/M ratio for all the dosimeters at each location is listed in the last column on the right in Tables 2.2-2.4. The average C/M ratios at location A1 (in front of the thermal shield) and at location A6 (at 3/4 wall thickness in the pressure vessel) are 0.91 ± 0.02 and 0.91 ± 0.04, respectively, for the calculations with the BUGLE-96 library. For the calculations with SAILOR-95 these ratios are 0.93 ± 0.01 and 0.92 ± 0.04, respectively. Thus, while a strong decrease in the C/M values with increasing distance from the core was typical for the calculations with the pre-ENDF/B-VI-based cross section libraries, no such decrease is observed in the calculations with the ENDF/B-VI-based libraries. Also, the variations of the C/M values for different dosimeters at the same location are small, as can be seen from the standard deviations of the average C/M values in Tables 2.2-2.4. This indicates that the shapes of the calculated spectra, in the energy range to which dosimeter responses are sensitive, are adequate (see also Appendix A).

2.3 REFERENCES

1. TORT-DORT Two- and Three-Dimensional Discrete Ordinates Transport Version 2.8.14, RSIC Computer Code Collection CCC-543, March 1994.

2. R. E. Maerker, "LEPRICON Analysis of the Pressure Vessel Surveillance Dosimetry Inserted into H. B. Robinson-2 During Cycle 9," *Nuc. Sci. Eng.* 96:263 (1987).

3. M. L. Williams, P. Chowdhury, and B. L. Broadhead, "DOTSYN: A Module for Synthesizing Three-Dimensional Fluxes in the LEPRICON Computer Code System," RSIC Peripheral Shielding Routine Collection PSR-277, March 1990.

4. W. A. Rhoades,"The GIP Program for Preparation of Group-Organized Cross Section Libraries," informal notes, November 1975, RSIC Peripheral Shielding Routine Collection PSR-75.

5. D. T. Ingersoll, et al., "Bugle-93: Coupled 47 Neutron, 20 Gamma-Ray Group Cross Section Library Derived from ENDF/B-VI for LWR Shielding and Pressure Vessel Dosimetry Applications," RSIC Data Library Collection, DLC-175, February 1994.

6. J. E. White, et al., "BUGLE-96: Coupled 47 Neutron, 20 Gamma-Ray Group Cross Section Library Derived from ENDF/B-VI for LWR Shielding and Pressure Vessel Dosimetry Applications," RSIC Data Library Collection, DLC-185, March 1996.

7. I. Remec and F. B. K. Kam, *An Update of the Dosimetry Cross-Section Data Base for the Adjustment Code LSL-M2*, ORNL/NRC/LTR-95/20, June 1995.

8. J. E. White, et al., "BUGLE-96: A Revised Multigroup Cross Section Library for LWR Applications Based on ENDF/B-VI Release 3," pp. 1071-1077, *Proc. of the American Nuclear Society 1996 Topical Meeting: Radiation Protection and Shielding*, North Falmouth, Mass., April 21-25, 1996.

3 CONCLUSION

Section 1 of this report describes the PCA benchmark and gives the dimensions, material compositions, and neutron source data necessary for benchmark analysis. The measured equivalent fission fluxes are also provided.

In Section 2, the analysis of the PCA benchmark is described. Calculations with the computer code DORT, based on the discrete ordinates method, were performed for three ENDF/B-VI-based multigroup libraries: BUGLE-93, SAILOR-95, and BUGLE-96. Excellent agreement of the calculated and measured equivalent fission fluxes was obtained. The arithmetic average C/M for all the measurements (a total of 31) was 0.93 ± 0.03 and 0.92 ± 0.03 for the SAILOR-95 and BUGLE-96 libraries, respectively. The BUGLE-93 library significantly overpredicted the thermal neutron fluxes and consequently the neptunium fission rates in water and air regions. The average C/M ratio, obtained with the BUGLE-93 library, for all the measurements except the neptunium measurements in the water and air regions (a total of 28 measurements) was 0.93 ± 0.03. No systematic decrease in the C/M ratios with increasing distance from the core was observed for any of the libraries used.

It is expected that the agreements of the calculations with the measurements, similar to those shown in this report, should typically be obtained when the discrete-ordinates method and ENDF/B-VI cross section libraries are used for the PCA benchmark analysis.

APPENDIX A

This appendix discusses several details regarding the PCA benchmark analysis and the evaluation of the results.

First, the effect of different dosimetry cross section sets is addressed. Reaction rates calculated with different cross sections sets are compared in Table A.1. In all cases, the same multigroup fluxes, obtained from the calculation with SAILOR-95, were used. As discussed in Section 2 of this report, reaction rates, which were compared with the measurements, were calculated with dosimetry cross sections from CROSS-95 and collapsed to the 47 groups with code FLXPRO, using the 640 groups reference spectrum (REF640B) and the calculated spectrum from location A4.[1] These reaction rates are listed in the column A of the Table A.1. The same procedure, using the calculated spectrum from location A1, was applied to generate a new dosimetry cross section set; the resulting reaction rates are compared in column B with the values from column A. The maximum differences are ~0.6% and are therefore not important. For the column C the cross sections were collapsed from CROSS-95 with the reference spectrum REF640B only. The reaction rates agree with the values in column A to approximately 0.6%, except for the ^{237}Np fission rates in water locations (e.g., A1–A3), where differences up to approximately 6% are observed. For the columns D and E the SAILOR-95 capsule-weighted and cavity-weighted dosimetry cross sections were used, respectively. The reaction rates obtained with these two sets are generally in good agreement with each other and with reaction rates obtained with other sets. Some differences (up to approximately 1.6%) were observed for the ^{27}Al(n,α) reaction. For the ^{115}In(n,n') reaction, SAILOR-95 dosimetry cross sections produced approximately 3-6% lower reaction rates than those given in the column A. For the ^{237}Np(n,f) reaction, the SAILOR-95 cross sections produced ~6% lower reaction rates than those in the column A at the locations in the water (A1-A3), while the agreements at the other locations are very good, typically to within 0.5%. The differences in the reaction rates, shown in Table A.1, indicate the variations that are caused by different dosimetry cross sections preparation and collapsing into the 47 groups energy structure. Observed differences for certain reactions (e.g., ^{237}Np(n,f) and ^{115}In(n,n')) are large enough to indicate that even this relatively trivial step in the calculational procedure deserves attention.

Several calculations were performed to evaluate the impact of different modeling approximations in the PCA benchmark analysis. Reaction rates from these calculations are compared with the results of the calculation performed as described in the Section 2 of this report. (This will be referred to in the following as the reference calculation.) In all calculations the SAILOR-95 library was used. The first modification considered the preparation of the source distribution. The point relative power densities, given in Table 1.5 of this report, were used directly (as-listed) to approximate the averages over one-ninth of the fuel-element cross section. The renormalization of the point values to the fuel-element relative powers given in Fig.1.11, which was done in the reference calculation, was

---

[1]The 640 groups reference spectrum (REF640B) consists of the Watt fission spectrum matched to 1/E spectrum at 0.5 MeV and to the Maxwellian thermal spectrum with the neutron temperature 323.16 K at 0.14 eV.

therefore omitted. Reaction rates from this calculation are compared to the reference calculation in column B of Table A.2. Differences are typically only a few tenths of a percent, and the maximum difference observed is only ~1%. It can therefore be concluded that the renormalization of the point power densities to the fuel-element relative powers is not necessary in the PCA benchmark analysis.

One of the requirements for the PCA core loading scheme was the quarter-core symmetry, which was closely approximated. However, as Fig.1.11 indicates, approximately 3% more power is generated in the quarter of the core farther from the aluminum window than in the quarter closer to the window. To quantify the impact of this, the calculations were repeated with a half-core model. For the quarter of the core farther from the aluminum window no data are available for the in-element power distributions; therefore, a flat distribution was assumed. The reaction rates from this calculation are compared with the reference calculation in column C of Table A.2. The calculation, which modeled a half-core, resulted in approximately 1.5% lower reaction rates than the reference calculation for all the reactions considered and all the locations. Again, the differences are small, and it is possible to conclude that using a one-quarter core model is satisfactory.

In the last calculation the effect of the ^{235}U fission spectrum representation was assessed. The ENDF/B-V ^{235}U fission spectrum [taken from ELXSIR (Ref.1)] was used instead of the ENDF/B-VI ^{235}U fission spectrum (as given in SAILOR-95). The calculation with the ENDF/B-V ^{235}U fission spectrum gave 0.3-1.3% higher reaction rates for all the locations and all the dosimeters considered except for the ^{27}Al (n,α) reaction, for which the calculation with ENDF/B-V fission spectrum gave 1.8-3.4% lower responses, as is shown in the column D of Table A.2.

It was shown that the calculated reaction rates (or equivalent fission fluxes) used in the PCA benchmark obtained by the three cross section libraries—BUGLE-93, SAILOR-95, and BUGLE-96— are generally in good agreement, with the exception of ^{237}Np and to some degree ^{238}U reaction rates calculated by BUGLE-93 at the locations in water. The differences between the BUGLE-93 reaction rates and those obtained with other two libraries show slow increases through the pressure vessel and reach approximately 6% in the void box behind the pressure vessel. However, if multigroup fluxes are compared, considerable differences between the BUGLE-93 and other two libraries are found not only in the thermal region, but also in the energy region from ~1 keV to ~1 MeV at the locations in the pressure vessel and behind. The differences reach approximately 20% at ~50 keV. These differences are probably caused by the different self-shielding of the iron and other steel components used in the preparation of the libraries. Because the reactions used in the PCA benchmark have zero or very low cross sections in the energy range mentioned above, the differences remain unnoticed when reaction rates only are compared.

REFERENCE

1. M. L. Williams et al., *The ELXSIR Cross-Section Library for LWR Pressure Vessel Irradiation Studies: Part of the LEPRICON Computer Code System*, EPRI NP-3654, Electric Power Research Institute, 1984.

Table A.1 Comparison of the reaction rates calculated with different sets of dosimetry cross-sections

Reaction	A*	B**	C***	D†	E‡
	Reaction rate	Difference from A			
	($s^{-1}atom^{-1}$)	(%)			
Position A1					
$^{27}Al(n,\alpha)$	5.18E-33	-0.1	-0.2	0.4	1.6
$^{58}Ni(n,p)$	5.84E-31	0.1	0	0.4	0.3
$^{103}Rh(n,n')$	3.87E-30	0.1	0.1		
$^{115}In(n,n')$	9.82E-31	0.2	0.1	-3.3	-3.7
$^{238}U(n,f)$	1.62E-30	0.3	0.2	0.1	-0.3
$^{237}Np(n,f)$	7.89E-30	0.1	-5.5	-5.6	-5.8
Position A2					
$^{27}Al(n,\alpha)$	6.62E-34	-0.1	-0.1	0.4	1.6
$^{58}Ni(n,p)$	6.21E-32	0.1	0	0.4	0.3
$^{103}Rh(n,n')$	4.41E-31	0.1	0.1		
$^{115}In(n,n')$	1.06E-31	0.2	0.2	-3.4	-3.9
$^{238}U(n,f)$	1.75E-31	0.3	0.2	0.1	-0.4
$^{237}Np(n,f)$	9.25E-31	0.1	-5.9	-5.9	-6.1
Position A3					
$^{27}Al(n,\alpha)$	3.04E-34	-0.1	-0.1	0.5	1.6
$^{58}Ni(n,p)$	2.38E-32	0	0	0.4	0.3
$^{103}Rh(n,n')$	1.44E-31	0.1	0.1		
$^{115}In(n,n')$	3.65E-32	0.1	0.1	-3.3	-3.7
$^{238}U(n,f)$	6.17E-32	0.3	0.2	0.1	-0.3
$^{237}Np(n,f)$	2.93E-31	0.1	-5.6	-5.7	-5.9
Position A4					
$^{27}Al(n,\alpha)$	6.84E-35	-0.1	-0.1	0.6	1.6
$^{58}Ni(n,p)$	5.34E-33	0.1	0	0.4	0.2
$^{103}Rh(n,n')$	5.56E-32	0.1	0.2		
$^{115}In(n,n')$	1.10E-32	0.2	0.3	-3.8	-4.7
$^{238}U(n,f)$	1.70E-32	0.4	0.4	0.1	-0.5
$^{237}Np(n,f)$	1.15E-31	0.1	0.1	0.2	-0.3

Table A.1 (continued)

	A*	B**	C***	D†	E‡
	Reaction rate	Difference from A			
Reaction	($s^{-1}atom^{-1}$)	(%)			
Position A5					
$^{27}Al(n,\alpha)$	2.71E-35	-0.1	-0.1	0.6	1.6
$^{58}Ni(n,p)$	2.09E-33	0.1	0.1	0.4	0.1
$^{103}Rh(n,n')$	2.99E-32	0.2	0.2		
$^{115}In(n,n')$	5.00E-33	0.3	0.3	-4.1	-5.2
$^{238}U(n,f)$	7.30E-33	0.5	0.5	0.1	-0.7
$^{237}Np(n,f)$	6.33E-32	0.1	0.2	0.4	-0.2
Position A6					
$^{27}Al(n,\alpha)$	1.02E-35	-0.1	-0.1	0.7	1.6
$^{58}Ni(n,p)$	7.68E-34	0.2	0.1	0.3	0
$^{103}Rh(n,n')$	1.49E-32	0.2	0.2		
$^{115}In(n,n')$	2.13E-33	0.3	0.4	-4.4	-5.7
$^{238}U(n,f)$	2.92E-33	0.6	0.6	0.1	-0.9
$^{237}Np(n,f)$	3.21E-32	0.2	0.2	0.4	-0.3
Position A7					
$^{27}Al(n,\alpha)$	3.10E-36	-0.1	-0.1	0.7	1.6
$^{58}Ni(n,p)$	1.97E-34	0.1	0.1	0.3	-0.1
$^{103}Rh(n,n')$	3.92E-33	0.2	0.2		
$^{115}In(n,n')$	5.43E-34	0.3	0.4	-4.5	-5.9
$^{238}U(n,f)$	7.31E-34	0.6	0.6	0	-0.9
$^{237}Np(n,f)$	8.67E-33	0.2	-1.1	-0.9	-1.7

* CROSS-95 dosimetry cross-sections collapsed by FLXPRO, using reference spectrum REF640B and calculated spectrum from location A4.

** Same as above note, but calculated spectrum from location A1 used.

*** CROSS-95 dosimetry cross sections collapsed by FLXPRO, using reference spectrum REF640B only.

† SAILOR-95 capsule-spectrum weighted dosimetry cross sections used.

‡ SAILOR-95 cavity-spectrum weighted dosimetry cross sections used.

Table A.2 Comparison of the reaction rates calculated using different modeling approximations

Reaction	A*	B**	C***	D†
	Reaction rate	Difference from A		
	($s^{-1}atom^{-1}$)	(%)		
Position A1				
$^{27}Al(n,\alpha)$	5.18E-33	0.4	-1.5	-1.8
$^{58}Ni(n,p)$	5.84E-31	0.1	-1.5	1.3
$^{103}Rh(n,n')$	3.87E-30	-0.0	-1.5	0.6
$^{115}In(n,n')$	9.82E-31	0.0	-1.5	0.7
$^{238}U(n,f)$	1.62E-30	0.0	-1.5	0.7
$^{237}Np(n,f)$	7.89E-30	-0.1	-1.5	0.3
Position A2				
$^{27}Al(n,\alpha)$	6.62E-34	1.1	-1.4	-2.2
$^{58}Ni(n,p)$	6.21E-32	0.4	-1.4	1.2
$^{103}Rh(n,n')$	4.41E-31	0.0	-1.5	0.8
$^{115}In(n,n')$	1.06E-31	0.1	-1.5	0.9
$^{238}U(n,f)$	1.75E-31	0.2	-1.4	0.9
$^{237}Np(n,f)$	9.25E-31	-0.0	-1.5	0.6
Position A3				
$^{27}Al(n,\alpha)$	3.04E-34	0.6	-1.3	-2.6
$^{58}Ni(n,p)$	2.38E-32	0.1	-1.4	1.2
$^{103}Rh(n,n')$	1.44E-31	-0.1	-1.4	1.0
$^{115}In(n,n')$	3.65E-32	-0.1	-1.4	1.1
$^{238}U(n,f)$	6.17E-32	-0.0	-1.4	1.0
$^{237}Np(n,f)$	2.93E-31	-0.2	-1.4	0.8
Position A4				
$^{27}Al(n,\alpha)$	6.84E-35	-0.3	-1.4	-2.8
$^{58}Ni(n,p)$	5.34E-33	-0.3	-1.4	1.1
$^{103}Rh(n,n')$	5.56E-32	-0.2	-1.5	1.0
$^{115}In(n,n')$	1.10E-32	-0.3	-1.5	1.1
$^{238}U(n,f)$	1.70E-32	-0.3	-1.4	1.0
$^{237}Np(n,f)$	1.15E-31	-0.2	-1.5	0.9

Table A.2 (continued)

Reaction	A*	B**	C***	D†
	Reaction rate	Difference from A		
	($s^{-1}atom^{-1}$)	(%)		
Position A5				
$^{27}Al(n,\alpha)$	2.71E-35	-0.0	-1.4	-3.0
$^{58}Ni(n,p)$	2.09E-33	-0.1	-1.4	1.0
$^{103}Rh(n,n')$	2.99E-32	-0.2	-1.5	0.9
$^{115}In(n,n')$	5.00E-33	-0.2	-1.4	1.0
$^{238}U(n,f)$	7.30E-33	-0.2	-1.4	0.9
$^{237}Np(n,f)$	6.33E-32	-0.2	-1.5	0.9
Position A6				
$^{27}Al(n,\alpha)$	1.02E-35	-0.1	-1.4	-3.2
$^{58}Ni(n,p)$	7.68E-34	-0.2	-1.4	0.9
$^{103}Rh(n,n')$	1.49E-32	-0.2	-1.5	0.9
$^{115}In(n,n')$	2.13E-33	-0.2	-1.4	1.0
$^{238}U(n,f)$	2.92E-33	-0.2	-1.4	0.9
$^{237}Np(n,f)$	3.21E-32	-0.2	-1.5	0.9
Position A7				
$^{27}Al(n,\alpha)$	3.10E-36	-0.2	-1.4	-3.4
$^{58}Ni(n,p)$	1.97E-34	-0.2	-1.4	0.8
$^{103}Rh(n,n')$	3.92E-33	-0.2	-1.5	0.9
$^{115}In(n,n')$	5.43E-34	-0.2	-1.4	1.0
$^{238}U(n,f)$	7.31E-34	-0.2	-1.4	0.9
$^{237}Np(n,f)$	8.67E-33	-0.2	-1.5	0.9

* Reference calculation, as described in Sect. 2 of this report. Reaction rates in column A are normalized to the PCA core source of one neutron per second.

** Same as above, but with renormalization of point powers to the fuel-element powers omitted.

*** One-half of the core modeled.

† ENDF/B-V (ELXSIR) ^{235}U fission spectrum used instead of the ENDF/B-VI (SAILOR-95).

NRC FORM 335 (2-89) NRCM 1102, 3201, 3202

U.S. NUCLEAR REGULATORY COMMISSION

BIBLIOGRAPHIC DATA SHEET

(See instructions on the reverse)

1. REPORT NUMBER (Assigned by NRC. Add Vol., Supp., Rev., and Addendum Numbers, if any.)

NUREG/CR-6454
ORNL/TM-13205

2. TITLE AND SUBTITLE

Pool Critical Assembly Pressure Vessel Facility Benchmark

3. DATE REPORT PUBLISHED

MONTH	YEAR
July	1997

4. FIN OR GRANT NUMBER

W6164

5. AUTHOR(S)

I. Remec, F.B.K. Kam

6. TYPE OF REPORT

7. PERIOD COVERED (Inclusive Dates)

8. PERFORMING ORGANIZATION – NAME AND ADDRESS (If NRC, provide Division, Office or Region, U.S. Nuclear Regulatory Commission, and mailing address; if contractor, provide name and mailing address.)

Oak Ridge National Laboratory
Oak Ridge, TN 37831- 6370

9. SPONSORING ORGANIZATION – NAME AND ADDRESS (If NRC, type "Same as above"; if contractor, provide NRC Division, Office or Region, U.S. Nuclear Regulatory Commission, and mailing address.)

Division of Engineering Technology
Office of Nuclear Regulatory Research
U.S. Nuclear Regulatory Commission
Washington, D. C. 20555-0001

10. SUPPLEMENTARY NOTES

C. J. Fairbanks, NRC Project Manager

11. ABSTRACT (200 words or less)

The pool critical assembly (PCA) pressure vessel wall facility benchmark (PCA benchmark) is described and analyzed in this report. Analysis of the PCA benchmark can be used for partial fulfillment of the requirements for the qualification of the methodology for pressure vessel neutron fluence calculations, as required by the U.S. Nuclear Regulatory Commission regulatory guide DG-1053. Section 1 of this report describes the PCA benchmark and provides all data necessary for the benchmark analysis. The measured quantities, to be compared with the calculated values, are the equivalent fission fluxes. In Section 2 the analysis of the PCA benchmark is described. Calculations with the computer code DORT, based on the discrete-ordinates method, were performed for three ENDF/B-VI-based multi-group libraries: BUGLE-93, SAILOR-95, and BUGLE-96. An excellent agreement of the calculated (C) and measures (M) equivalent fission fluxes was obtained. The arithmetic average C/M for all the dosimeters (total of 31) was 0.93 ± 0.03 and 0.92 ± 0.03 for the SAILOR-95 and BUGLE-96 libraries, respectively. The average C/M ratio, obtained with the BUGLE-93 library, for the 28 measurements was 0.93 ± 0.03 (the neptunium measurements in the water and air regions were overpredicted and excluded from the average). No systematic decrease in the C/M ratios with increasing distance from the core was observed for any of the libraries used.

12. KEY WORDS/DESCRIPTORS (List words or phrases that will assist researchers in locating the report.)

Pool critical assembly
Reactor pressure vessel
Neutron dosimetry
Neutron transport calculations
ENDF/B-VI
Qualification of the calculational methodology

13. AVAILABILITY STATEMENT

Unlimited

14. SECURITY CLASSIFICATION

(This Page)
Unclassified

(This Report)
Unclassified

15. NUMBER OF PAGES

16. PRICE

NRC FORM 335 (2-89)